Final Report

NASA Project Title: **SAR Investigations of Glaciers in Northwestern North America**

Grant No.: NAGW-2827 (NRA 91-OSSA-07)

Time Period: 1 December 1991 - 31 May 1994

Principal Investigator: Dr. Craig S. Lingle
Geophysical Institute
University of Alaska Fairbanks
P.O. Box 757320
Fairbanks, AK 99775-7320
Tel. 907-474-7679
Fax 907-474-7290
E-mail: clingle@iias.images.alaska.edu

Co-Investigator: Dr. William D. Harrison
- same address -
Tel. 907-474-7706
Fax 907-474-7290
E-mail: harrison@dino.gi.alaska.edu

NASA Technical Officer: Dr. Robert H. Thomas
Polar Programs Manager
Science Division
Office of Mission to Planet Earth
NASA Headquarters
Code YSG
Washington, D.C. 20546-0001

Date: 25 August 1995

Project Summary

The objective of this project was to investigate the utility of satellite synthetic aperture radar (SAR) imagery for measurement of geophysical parameters on Alaskan glaciers relevant to their mass balance and dynamics, including: (i) the positions of firn lines (late-summer snow lines), (ii) surface velocities on fast-flowing (surging) glaciers, and also on slower steady-flow glaciers, and (iii) the positions and changes in the positions of glacier termini. Preliminary studies of topography and glacier surface velocity with SAR interferometry have also been carried out. This project was motivated by the relationships of multi-year to decadal changes in glacier geometry to changing climate, and the probable significant contribution of Alaskan glaciers to rising sea level.

Note: Additional funding for this project was obtained from the National Science Foundation (Lingle, 1993) and Cray Research, Inc. (Lingle, 1994). Work supported by these sources is treated, below, as part of the same project.

The results are summarized on pp. 2-6. Conclusions regarding the utility of spaceborne SAR for glaciological research are on p. 7. The figures (13) are at the end of this report.

Results

(i) Identification of firn lines on Alaskan glaciers.

A year-long time series of SAR images of Black Rapids Glacier—which is a 45 km-long glacier occupying a section of the Denali fault in the east-central Alaska Range—was processed, along with SAR imagery of other glacierized areas in Alaska and Yukon, including a year-long time series of SAR images of Nabesna Glacier on Mt. Wrangell, in the Wrangell Mountains. Black Rapids Glacier was chosen as the primary focus because it has a 20-year time series of field measurements of mass balance and equilibrium line altitude (ELA), as well as other quantities including surface elevation, ice thickness, velocity, near-surface temperatures, and stream discharge. This program of field measurements has been carried out by glaciologists from the U.S. Geological Survey (USGS) and Geophysical Institute in Fairbanks, and the University of Washington in Seattle. SAR image processing was carried out by Ms. K. Ahlnäs, of Geophysical Institute.

We conclude that firn lines on glaciers can be identified and mapped using spaceborne C-band SAR imagery. (Note: 'Firn line' means the maximum late summer snow line, not the down-glacier edge of superimposed ice at the end of the balance year. The latter is the 'equilibrium line.') This is most easily done using imagery acquired during winter, when the complicating effects of surface meltwater are not present. The firn lines—which are clearly recognizable beneath the radar-transparent dry snow—appear as slightly diffuse boundaries separating the specular ice of ablation areas from the radar-bright frozen firn of accumulation areas. The correspondence between this boundary and the firn line was established by comparison to the time series of equilibrium line altitudes (ELA's) estimated from field data by Heinrichs et al. (1995). Additional field verification of the SAR-derived position of the firn line was obtained with an automatic camera, which was mounted during summer 1993 at a site on the valley wall overlooking the upper glacier, including the area of the firn line. The resulting time-series of photos showed the transient snow line retreating to its firn-line position at the end of summer. Subsequently the position of the firn line was converted to geographic coordinates, using the method of Harrison et al. (1992), by Mr. M. Tamstorf (a summer exchange student from Copenhagen working with Dr. W. Harrison). The position of the firn line mapped from the photos was found to approximate the position of the SAR-derived firn line, and the position of the ELA estimated from field data by Heinrichs et al. (1995). (There can be—and often is, on interior glaciers in Alaska and the Yukon Territory—an area of superimposed ice between the firn line and the ELA. Superimposed ice occurs less often on coastal glaciers. We do not have evidence that SAR can distinguish between the exposed glacier ice of the ablation area and superimposed ice.)

The position of a transient mid-summer snow line on Black Rapids Glacier, appearing in a SAR image acquired 17 July 1992 by ERS-1, was verified by direct observation from a small airplane by Dr. W. Harrison on that date. The flight, piloted by Dr. K. Echelmeyer, was in conjunction with summer field work on the glacier. The position of the transient snow line was drawn on a USGS map, using visual comparison to recognizable topographic features, then later compared to the apparent position of the transient snow line appearing in the SAR image. The two were indistinguishable.

The capability of SAR for mapping firn lines effectively circumvents the difficulty long associated with use of visible imagery and aerial photography for that purpose, which is that an image or photograph must be acquired at the difficult-to-predict end of the balance year. See *Figure 1.*

(ii) Terrain correction of full-resolution SAR imagery, and measurement of the initiation and development of a large glacier surge.

Terrain-correction is accomplished using the software originally developed by Wivell et al. (1992). This software has been adapted to run on the T3D massively parallel processor of the Arctic Region Supercomputing Center (ARSC) by Mr. T. Logan, of the Alaska SAR Facility, under a project funded by Cray Research, Inc., for which Dr. S. Li, of Geophysical Institute, was the principal investigator. Consequently, it is now computationally feasible to terrain correct entire full-resolution images, not just relatively small subscenes.

A difficulty that arises with respect to terrain correction of full-resolution imagery is that the rectified images necessarily have the same resolution as the underlying digital elevation model (DEM). The highest resolution U.S. Geological Survey (USGS) DEM available for most of Alaska is defined on a 3 arc-second of latitude by 6 arc-second of longitude (approximately 90 m x 90 m) grid (USGS, 1990). Full-resolution SAR images, however, have 12.5 m pixels and a nominal resolution of 30 m. It is thus necessary to interpolate the DEM onto a 30 m grid to avoid unacceptable loss of resolution. This is done via the optimum interpolation method of kriging (e.g., Isaaks and Srivastava, 1989), using software developed by Dr. V.A. Voronina (Voronina and Lingle, 1994a). Kriging of 90 m DEM's onto 30 m grids is computationally time-consuming, so Dr. Voronina developed this software to run on the ARSC Cray system.

It was found that interpolation of the 90 m Alaska DEM onto a 30 m grid yields greatly-improved results with terrain correction of full-resolution SAR imagery. This approach was employed by Roush, Lingle, and Guritz (submitted) for terrain correction of subscenes of the lower Bering Glacier during its 1993-'94 surge. The location of this area is shown by the map in *Figure 2* (it is a sub-area of the box is the southwest corner).

(iia) The 1993-'95 surge of Bering Glacier. *Figure 3* is a SAR image of Bering Glacier and Bagley Icefield, in the Chugach Mountains of Southcentral Alaska, terrain corrected at low resolution using the 90 m DEM for this region. With a total area including tributaries of 5,200 km^2 (Molnia, 1993), the Bering Glacier-Bagley Icefield system is the largest glacier in North America, and in the world outside Antarctica and Greenland. As noted in the caption, the image was acquired by ERS-1 on 9 August 1993, roughly 4 months after the start of the surge (Lingle et al., 1994). The surge front reached the terminus and Vitus Lake (lower left) during late-August and early-September '93. Subsequently the surge continued until late summer '94, then stopped. Termination probably coincided with a violent and sustained outburst of subglacial water that occurred at the end of July. The surge re-started in spring '95 (Molnia, 1995).

Figure 4 shows successive positions of the surge front during propagation to the terminus, measured by Mr. J.J. Roush with sequential ERS-1 SAR subscenes acquired on the dates indicated in the figure. *Figure 5* shows successive positions of the terminus during advance, also measured by Mr. Roush using SAR subscenes acquired on the dates indicated. The results of this work are summarized in the abstract from Roush, Lingle, and Guritz (submitted, 1994a):

> "Sequential ERS-1 C-band synthetic aperture radar (SAR) images of the 1993-'94 surge of Bering Glacier, Alaska, suggest that the surge began between late March and late April 1993. Subsequently the surge front propagated down-glacier at a mean velocity of 90 m/day between 19 May and 25 August, reaching most of the 34 km perimeter of the terminus by and shortly after 25 August. Since then the calving terminus has advanced rapidly into proglacial Vitus Lake, at a maximum rate, in its central area, of 19 m/day between 9 August and 18 October 1993. The mean rate of advance across the entire width of the terminus was 11 m/day during the same time period. The advancing surge front consisted of a distributed region

of undulations and bulges on the glacier surface having heights, estimated from the SAR data, of 40 to 110 m and widths varying from about 0.7 to 1.5 km. The measurements were made using terrain corrected, geocoded and coregistered images."

A time-lapse movie of the down-glacier propagation of the surge front and subsequent advance of the terminus, showing the development and evolution of fast flow, was also produced by Mr. Roush and Mr. R.M. Guritz from a sequence of 11 ERS-1 SAR image subscenes, extending from 22 November 1992 through 18 October 1993 (Roush et al., 1994b). More recently, an additional 4 subscenes were added extending through 1 June 1994, by Dr. M. Roth (of ARSC), Mr. Guritz, and colleagues. Sound and narration are included. Copies of this video tape can be obtained from the authors.

(iii) SAR measurement of velocity on a large surging glacier: Feature matching, kriging, and principal strain rates.

Surge fronts propagate more rapidly than the flow velocity of the ice. A simple conservation of volume argument (Kamb et al., 1985; Raymond et al., 1987) can be used to show that in the case of the lower Bering Glacier, surge front propagation velocities in the range 75 to 112 m/day may have corresponded to ice-flow velocities of the order of 9 to 14 m/day (Roush et al., submitted, 1994a). These estimates were made using USGS radar measurements of pre-surge depth to bedrock (Molnia, 1993).

Ice velocity vectors on Bering Glacier were measured by Mr. D.R. Fatland, using two complex images acquired from exact repeat orbits during the 35-day orbit phase of ERS-1—i.e., the images were separated by 35 days—before and after the surge front reached the terminus. The images were not terrain corrected, in order to preserve resolution. Power-domain averaging over 5 pixels in the azimuth direction resulted in pixels that were 20 m (azimuth) by 7.9 m (range). The slant-range pixels correspond to about 20 m in ground-range, so the aspect ratio was close to one.

The velocity vectors were determined by coregistering the two images, then measuring the displacements of features that could be recognized in both, avoiding crevasses that were deforming so rapidly that their dimensions changed noticeably during the 35-day time interval. The measured velocities tend to be concentrated along the northern and northwestern sides of the glacier, where tributaries entering from the Khitrov Hills have brought in rock debris resulting in recognizable surface patterns. Increased fracturing of the glacier surface as it entered the piedmont lobe permitted measurement of a great many displacement vectors on the lower glacier. The scale at lower right shows that a vector length of 4 mm represents a velocity of 10 m/day. Measured velocity vectors having x and y components comparable to 10 m/day have an uncertainty of about 0.4 m/day (3%), due to the finite dimensions of the pixels.

Figure 6 shows the resulting velocity field, kriged by Dr. Voronina onto a 1 km square grid within the irregular domain defined by the boundaries of the glacier. The location of this area is shown by the box in the southwest corner (bottom-left) of the map in Figure 2. The spatial structure in the data was quantified by computing variograms for the orthogonal components of the vectors. The x and y components were then kriged independently. The measurement errors resulting from finite pixel size were propagated through the kriging equations, and the additional (generally larger) errors caused by the spatial distances over which the velocities were interpolated were also computed. The gridded velocity vectors retained in Figure 6 are those for which the total error was less than 30% of the velocity.

Figure 7 shows the horizontal principal components of the strain-rate tensor, computed by Dr. Voronina from the orthogonal gradients of the kriged velocity vectors. The errors computed for the velocities were propagated through the strain-rate equations. Only the strain

rates with errors less than 45% are shown in Figure 7. Compression is indicated by red; extension by green. The scale at lower right shows the distance corresponding to a (very large) strain rate of 0.01 per day, which is equivalent to 3.7 per year. Many of the strain rates on the piedmont lobe near the terminus are comparable to this or larger, particularly toward the western (left) side. Note that on the lower glacier the surge forced thickening, which implies extensive vertical strain rates, so it is possible for both of the horizontal principal components to be compressive. Figure 7 shows that intense compressive strain rates along the entire perimeter of the terminus were caused by the arrival of the surge front. *Icebergs from the heavily fractured terminus filled Vitus Lake shortly after this image-pair was acquired.*

(iv) Satellite Radar Interferometry: Surface velocity on Alaskan icefields, and DEM's.

The methods and technology of aircraft and satellite radar interferometry (SRI) were developed at NASA's Jet Propulsion Laboratory, and have been described by Zebker and Goldstein (1986), Massonnet et al. (1993), Goldstein et al. (1993), and Zebker et al. (1994), among others. Here at Geophysical Institute, Mr. Fatland has successfully synthesized interferograms showing, primarily, the component in the radar line-of-sight direction of the velocity field on Bagley Icefield and its tributaries, in the Chugach and St. Elias Mountains of Southcentral Alaska, before and during the recent surge of Bering Glacier (Fatland, 1994; Fatland and Lingle, 1994; 1995a,b,c). Mr. Fatland has also used SRI to synthesize a preliminary DEM of an area on the north slope of Alaska.

(iva) Topography versus surface motion. An interferogram of 'fixed topography' represents elevation differences throughout the area—combined with the effects of errors, which are discussed briefly below. Alternatively, an interferogram of moving surfaces—such as glaciers or an ice sheet—would represent mostly the component of motion in the radar line-of-sight direction, if the transverse baseline between the satellite positions at the two acquisition times were sufficiently small. 'Small' means of the order of a few meters to tens of meters. If the baseline were relatively large, i.e., of the order of 100 to 1,000 m, the resultant interferogram would include both surface motion and topographic information. For repeat passes during the 3-day orbit cycles of ERS-1, the latter situation was more common than the former.

(ivb) Error sources. There are primarily two sources of error, given coregistration between two images that is adequately 'tight' to yield an interferogram, combined with changes in surface dielectric properties and surface motion not so large as to cause decorrelation. (1) Phase noise. This is a form of random error that increases the difficulty of phase unwrapping; that is, conversion of the pixel-to-pixel phase differences into elevation differences or surface displacements throughout the interferogram. (2) Baseline error. This is due to uncertainty in the length of the transverse baseline—which must be inferred—between the two positions of the satellite at the acquisition times. The latter results in systematic error, which is expressed as fringes that translate, after phase unwrapping, into a plane of constant slope superimposed on the quantity of interest (topography and/or surface motion). Discussions of these error sources can be found in the literature; they are not discussed further in this report—except to note that phase noise is relatively manageable, while the more serious baseline error requires 'deramping,' which is, in essence, a trial-and-error interative approach.

(ivc) Figure locations. Relative to the map in Figure 2, the location of the interferogram shown in *Figure 8*—which includes a segment of the unglacierized Chitina Valley—is just off the map to the north and west (top-left). The valley discharging Tana Glacier (top-center of map) is in the southwest (lower left) corner of Figure 8. The location of the interferogram shown in *Figure 9* (Bagley Icefield) is shown by the box at top-right in Figure 2. The interferograms shown in *Figures 10 and 11* are centered in the area of diverging ice flow indicated by the arrows just left (west) of the box. Figures 10 and 11 overlap the left edge of the box.

(ivd) Case 1: Valley-bottom topography versus a moving icefield. Chitina Valley, which has a broad 'flat' bottom with downstream slope roughly comparable to Bagley Icefield, can be seen in Figure 8 to be characterized by broad fringes which represent the effects of changing elevation along the valley bottom.

Bagley Icefield (Figure 9) can be seen to be characterized by closely-spaced fringes. Comparison of Figure 9 to the broadly-spaced 'topographic fringes' of Figure 8 indicates that the fringes on Bagley Icefield represent, primarily, the component of glacier motion in the radar line-of-sight direction, not the effects of topography. This interferogram was synthesized from SAR images acquired 4 and 7 February 1994, during the surge of Bering Glacier. Changes in the fringe pattern at the western (left) end of the icefield, relative to an interferogram of this area synthesized from images acquired in January 1992, prior to surge onset, show that the surge propagated up-glacier into Bagley Icefield as well as down-glacier to the terminus. Note that the the western (left) side of the interferogram in Figure 9 overlaps with the eastern (right) sides of the interferograms in Figures 10 and 11.

(ive) Case 2: Change in ice flow within Bagley Icefield. The area where Bering Glacier descends from Bagley Icefield (diverging arrows in the map of Figure 2) is shown in Figures 10 and 11. Figure 10 was synthesized from an image-pair acquired during January 1992, prior to surge onset. Figure 11 was synthesized from an image-pair acquired during February 1994, while the surge was in progress. Both pairs were separated by 3 days. Bering Glacier, which descends from below-center towards lower left, is decorrelated in both cases due to flow too rapid for interferometry. The change in the Bagley Icefield fringe pattern at lower-right (southwest corner of image)—with increased decorrelation indicating faster flow—shows, however, that longitudinal stretching caused the surge to propagate up-glacier into the icefield. Direct observation of this area from a small airplane in June 1993 (Lingle et al., 1993a) yielded a conclusion that at that time, the surge had not propagated upstream to the upper Bering Glacier (nor had it reached the terminus, although it was in progress on the lower glacier). The interferograms of Figures 10 and 11 thus provide evidence that the surge propagated in both directions.

(ivf) Case 3: A digital elevation model from interferometry: The Alaska north slope. Figures 12 and 13 are an example—unrelated to the Bering Glacier surge, discussed above—of the use of interferometry to synthesize a DEM of an area consisting of 'fixed topography;' that is, without moving glaciers. This work, carried out by Mr. Fatland, is a preliminary result. The area, about 40 km top-to-bottom by 50 km left-to-right, is located on the central north slope of Alaska within a region characterized by gradual tundra-covered slopes and low hills, dissected by an extensive system of rivers and lakes. The Sagavanirktok River, which flows north (right), follows the prominent discontinuity crossing the interferogram (Figure 12), which was synthesized from images acquired 26 and 29 September 1991, during the commissioning phase of ERS-1. Each of the color bands corresponds to an elevation difference of roughly 10 m. Control points within the corresponding 1:250,000 USGS topographic map were employed for ground control in the derivation of the DEM shown in Figure 13. A thorough error analysis has not yet been carried out, but analogous work by others (at the time of this work), at the Jet Propulsion Laboratory, suggested that the RMS error of the DEM might be approximately 15 m.

This work demonstrates the feasibility of synthesizing DEM's from repeat-pass interferometry, while emphasizing the importance of independent ground control for calibration of the fringes. It is important to note that there is no absolute relationship between the interference fringes shown in Figure 12 and the DEM shown in Figure 13. If the transverse baseline between the repeat passes yielding the SAR images employed for synthesis of Figure 12 were different, the entire fringe pattern would be expanded or contracted.

Conclusions: Utility of Spaceborne SAR for Glaciological Research

(1) *Mass balance, I.* Spaceborne C-band synthetic aperture radar (SAR) is suitable for mapping of firn line positions on glaciers. Mapping of firn lines in terms of geographic coordinates (latitude-longitude, and/or UTM) will be possible using terrain-corrected images. Winter imagery is most effective, due to absence of surface meltwater, particularly on interior glaciers. On coastal glaciers, the positions of firn lines are more ambiguous in winter imagery, probably due to deeper snow and warmer termperatures, combined with melting and refreezing.

(2) *Mass balance, II.* Spaceborne SAR is also suitable for mapping of the positions of glacier termini, in cases where the termini are sufficiently clean (i.e., clear of rock debris) to be identifiable. Full-resolution SAR images, terrain-corrected using a DEM interpolated to 30 m, can be used to map termini to an accuracy of about $\pm$ one-half pixel ($\pm$ 15 m), which suggests that changes greater than roughly 20-25 m in the positions of termini should be detectable.

(3) *Surging glacier dynamics*. Spaceborne SAR has proven to be an effective tool for study of the dynamics of a large Alaskan glacier during a major surge. By implication, it is very likely to be an effective tool for study of the dynamics of fast-flowing tidewater glaciers, and changes in the positions of the termini of tidewater glaciers due to iceberg calving.

(3) *Glacier surface velocity (feature-matching).* Surface velocities can be measured on glaciers having features that are recognizable in sequential SAR images, although care must be taken to select features that are not deforming so rapidly, in addition to translating, that their dimensions change significantly between image acquisitions. Preliminary results from the lower ablation area of Bering Glacier, during its recent surge, suggest that this may be best accomplished using complex full-resolution slant-range images, which have smaller pixels and generally better resolution than 'conventional' full-resolution images.

(4) *Glacier surface velocity (cross-correlation).* Measurement of glacier surface velocities via cross-correlation of sequential SAR images was investigated (Voronina and Lingle, 1994), using software developed by Bindschadler and Scambos (1991) for use with Landsat TM imagery. This methodology was found to work, in a mechanical sense, with full-resolution SAR imagery. The software has been improved, in a computational sense, and adapted to run on the Cray system of the Arctic Region Supercomputing Center. It is now feasible to carry out cross-correlation of entire full-resolution SAR images. This method has been employed for preliminary measurement of surface velocities on Malaspina Glacier, which is a large-area piedmont glacier on the coast of Southcentral Alaska. The results suggest that this approach will be effective, given images from an exact-repeat orbit, adequately 'tight' coregistration, a sufficient time interval between the images, and a glacier surface adequately 'rough' for features to be recognizable, in a statistical sense.

(5) *Satellite radar interferometry (SRI).* SRI has been implemented successfully in the heavily glacierized, heavy precipitation, mountainous and tectonically-active environment of Southcentral and Southwestern Alaska, and on the north slope of Alaska near the arctic coast. This new technology has proven to be effective for synthesis of high quality digitral elevation models and for measurement (in preliminary form) of surface velocities on glaciers, in spite of difficulties due to relatively fast glacier flow, changing surface dialectric properties caused by changing meteorological conditions, and precipitous terrain in these challenging regions. The outlook is favorable for successful separation of 'topographic effects' from 'surface motion effects,' given interferogram pairs synthesized from repeated image pairs along exact repeat orbits. Patience and a certain amount of 'good fortune' are required for identification of suitable image pairs, and the difficulties are non-trivial in getting from interferograms to geophysical products such as glacier surface velocity, DEM's, or both (or volcano deformation, which is of

great interest to volcanologists). SRI shows every indication, however, of leading to breakthroughs in glacier research, as well as in solid earth geophysics. The possibilities that will be opened up by the data set that will result from the ERS-1 and ERS-2 tandem mission can reasonably be described as 'very large.'

(v) Papers resulting from this project.

Lingle, C.S., A. Post, U.C. Herzfeld, B.F. Molnia, R.M. Krimmel, and J.J. Roush. 1993a. Bering Glacier surge and iceberg-calving mechanism at Vitus Lake, Alaska, U.S.A. (correspondence). *Journal of Glaciology,* 39(133), 722-727.

Roush, J.J., C.S. Lingle, and R.M. Guritz. The surge of Bering Glacier, Alaska, observed with satellite synthetic aperture radar. Submitted to *Journal of Glaciology,* 1994a.

Lingle, C.S., W.D. Harrison, K. Ahlnäs, and T.A. Heinrichs. Year-round observations of an Alaskan glacier with spaceborne synthetic aperture radar. In preparation.

(vi) Contributions to European Space Agency Report.

Roush, J.J., C.S. Lingle, and R.M. Guritz. 1995. SAR subscenes (3) showing propagation of surge front and advance of terminus during surge of Bering Glacier, Alaska. Figure 5.14a,b,c, p. 96, in: *New Views of the Earth: Scientific Achievements of ERS-1,* ESA SP-1176/1 (162 pp).

Fatland, D.R., and C.S. Lingle. 1995b. SAR Interferogram showing motion of Bagley Icefield and tributaries during surge of Bering Glacier, Alaska. Figure 5.15, p. 97, in: *New Views of the Earth: Scientific Achievements of ERS-1,* ESA SP-1176/1 (162 pp).

(vii) Contribution to Report to National Research Council.

Fatland, D.R., and C.S. Lingle. 1995c. SAR Interferogram showing motion of Bagley Icefield and tributaries during surge of Bering Glacier. Figure 5-10, p. 5-18, in: *Spaceborne Synthetic Aperture Radar: Current Status and Future Directions. A report to the Committee on Earth Sciences, Space Studies Board, National Research Council,* NASA Technical Memorandum 4679.

(viii) Time-lapse movie of glacier surge, from SAR imagery.

Roush, J.J., C.S. Lingle, and R.M. Guritz. 1994. The 1993-'94 surge of Bering Glacier, Alaska, observed with ERS-1 synthetic aperture radar imagery. Time-lapse movie (unpublished), available from the authors on VHS video tape.

(ix) Presentations at regional, national, and international symposia

Lingle, C.S., W.D. Harrison, K. Ahlnäs, and T.A. Heinrichs. 1992. Observations of Black Rapids Glacier, Alaska Range, with synthetic aperture radar. Presented at *International Symposium on Remote Sensing of Snow and Ice,* International Glaciological Society, at Boulder, Colorado, May 17-22.

Lingle, C.S., W.D. Harrison, and K. Ahlnäs. 1992. Observations of glaciers in the St. Elias Mountains, Alaska-Yukon Territory, with synthetic aperture radar. (Invited paper.) *43rd AAAS Arctic Science Conference,* Valdez, Alaska, Sep. 8-11.

Ahlnäs, K., C.S. Lingle, W.D. Harrison, T.A. Heinrichs, and K.A. Echelmeyer. 1992. Identification of late-summer snow lines on glaciers in Alaska and the Yukon Territory with ERS-1 SAR imagery. *Eos, AGU Fall Meeting Supplement,* 73(43), 204, Oct. 27.

Lingle, C.S., W.D. Harrison, K. Ahlnäs, T.A. Heinrichs, and J.J. Roush. 1993b. Observation of Alaskan glaciers with ERS-1 synthetic aperture radar. *ASF SAR Users Meeting,* 27-29 July, Seattle, Washington.

Roush, J.J. 1993. Satellite imaging of Bering Glacier: Investigation of a surging glacier using terrain corrected synthetic aperture radar. *Eos, AGU Fall Meeting Supplement,* 74(43), 74, Oct. 26.

Voronina, V.A., and C.S. Lingle. 1994a. Resolution enhancement of digital elevation models for terrain correction of SAR imagery. *Third Circumpolar Symposium on Remote Sensing of Arctic Environments,* Fairbanks, Alaska, May 16-20.

Fatland, D.R. 1994. Glacier surface motion analysis using SAR interferometry. *Third Circumpolar Symposium on Remote Sensing of Arctic Environments,* Fairbanks, Alaska, May 16-20.

Fatland, D.R., and C.S. Lingle. 1994. The surface velocity field on Bagley Icefield, Alaska, before and during the 1993-'94 surge of Bering Glacier, from ERS-1 SAR Interferometry. (Invited paper.) *Eos, AGU Fall Meeting Supplement,* 75(44), 62, Nov. 1.

Roush, J.J., C.S. Lingle, and R.M. Guritz. 1994c. The surge of Bering Glacier, observed with sequential ERS-1 synthetic aperture radar imagery. (Invited paper.) *Eos, AGU Fall Meeting Supplement,* 75(44), 63, Nov. 1.

Lingle, C.S., J.J. Roush, and D.R. Fatland. 1994. Time of onset of the 1993-'94 surge of Bering Glacier, Alaska, and effect on iceberg calving of surge arrival at the terminus (Invited paper). *Eos, AGU Fall Meeting Supplement,* 75(44), 64, Nov 1.

Voronina, V.A., and C.S. Lingle. 1994. Investigation of surface velocity measurement on Malaspina Glacier, Alaska, with sequential ERS-1 SAR imagery (revised title). *Eos, AGU Fall Meeting Supplement,* 75(44), 224, Nov 1.

Fatland, D.R., and C.S. Lingle. 1995c. Elements of digital elevation model generation using spaceborne radar interferometry. *91st Annual Meeting of Cordilleran Section of Geological Society of America,* Fairbanks, Alaska, May 24-26.

Fatland, D.R., V.A. Voronina, and C.S. Lingle. 1995. Velocity and strain rates on lower Bering Glacier, Alaska, during the 1993-'94 surge, from ERS-1 spaceborne SAR imagery. *91st Annual Meeting of Cordilleran Section of Geological Society of America,* Fairbanks, Alaska, May 24-26.

Roush, J.J., and C.S. Lingle. 1995. Synthetic aperture radar imaging of the 1993-'94 surge of Bering Glacier, Alaska: Application of terrain corrected SAR to a problem in glacier mechanics. *91st Annual Meeting of Cordilleran Section of Geological Society of America,* Fairbanks, Alaska, May 24-26.

Lingle, C.S., D.R. Fatland, R.M. Guritz, J.J. Roush, and V.A. Voronina. 1995. Satellite Synthetic Aperture Radar: Interferometry, DEM's, Terrain Correction, and Alaskan Glacier and Volcano Studies. (Invited lecture.) *17th Canadian Symposium on Remote Sensing,* 13-15 June, Saskatoon, Saskatchewan, Canada.

References (cited in text, but not in above lists)

Bindschadler, R.A., and T.A. Scambos. 1991. Satellite-image-derived velocity field of an Antarctic ice stream. *Science,* 252, 242-246.

Goldstein, R.M., H. Engelhardt, B. Kamb, and R.M. Frolich. 1993. Satellite radar interferometry for monitoring ice sheet motion: Application to an Antarctic ice stream. *Science,* 262, 1525-1530.

Harrison, W.D., K.A. Echelmeyer, D.M. Cosgrove, and C.F. Raymond. 1992. The determination of glacier speed by time-lapse photography under unfavorable conditions. *J. Glaciol.,* 38(129), 257-265.

Heinrichs, T.A., L.R. Mayo, R.S. March, and D.C. Trabant. 1995. Observations of surge-type Black Rapids Glacier, Alaska, during a quiescent period, 1972-92. U.S. Geological Survey Open-File Report 94-512.

Isaaks, E.H., and Srivastava, R.M. 1989. *Applied Geostatistics.* Oxford University Press, New York.

Kamb, B., C.F. Raymond, W.D. Harrison, H. Engelhardt, K.A. Echelmeyer, N. Humphrey, M.M. Brugman, and T. Pfeffer. 1985. Glacier surge mechanism: 1982-1983 surge of Variegated Glacier, Alaska. *Science,* 227, 469-479.

Lingle, C.S. 1993. Surface velocity measurements on Bering Glacier during surge. Small Grant for Exploratory Research (one year), funded by NSF Glaciology Program, 15 Sept. 1993-28 Feb. 1995.

Lingle, C.S. 1994. Measurement of surface velocity and elevations with synthetic aperture radar imagery: Application to glaciers and the solid earth. Grant funded by Cray Research, Inc., 1993 University Research and Development Grant Program, 22 March 1994-21 March 1995.

Lingle, C.S., A. Post, U.C. Herzfeld, B.F. Molnia, R.M. Krimmel, and J.J. Roush. 1993. Bering glacier surge and icberg-calving mechanism at Vitus Lake, Alaska, U.S.A. (correspondence). *J. Glaciol.,* 39(133), 722-727.

Massonnet, D., M. Rossl, C. Carmona, F. Adragna, G. Peltzer, K. Felgl, and T. Rabaute. 1993. The displacement field of the Landers earthquake mapped by radar interferomery. *Nature,* 364(6433), 138-142.

Molnia, B. 1993. Major surge of the Bering Glacier. *Eos,* 74(29), 321-322.

Molnia, B. 1995. Bering Glacier resumes its surge. *Eos,* 76(29), 291.

Raymond, C., T. Jóhannesson, and T. Pfeffer. 1987. Propagation of a glacier surge into stagnant ice. *J. Geophys. Res.,* 92(B9), 9037-9049.

U.S. Geological Survey. 1990. *Digital Elevation Models: Data Users Guide 5,* National Mapping Program Technical Instructions, 51 pp.

Wivell, C.E., D.R. Steinwand, G.G. Kelly, and D.J. Meyer. 1992. Evaluation of terrain models for the geocoding and terrain correction of synthetic aperture radar (SAR) images. *IEEE Trans. Geosci. and Remote Sensing,* 30(6), 1137-1143.

Zebker, H., and R. Goldstein. 1986. Topographic mapping from interferometric synthetic aperture radar observations. *J. Geophys. Res.,* 91, 4993-4999.

Zebker, H.A., P.A. Rosen, R.M. Goldstein, A. Gabriel, and C.L. Werner. 1994. On the derivation of coseismic displacement fields using differential radar interferometry: The Landers earthquake. *J. Geophys. Res.,* 99(B10), 19617-19634.

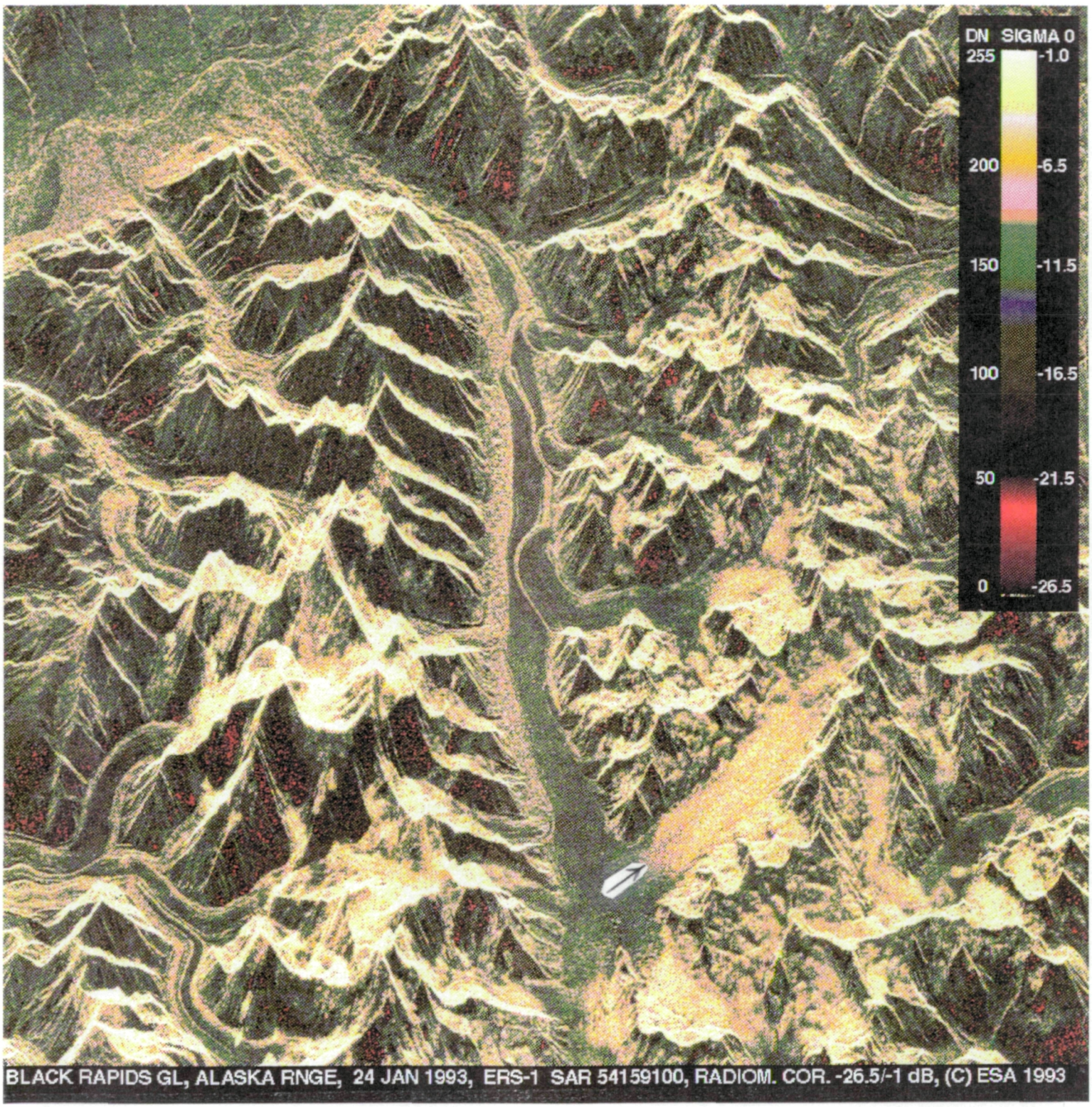

Fig. 1. Black Rapids Glacier, Alaska Range, on 24 January 1993. This area is located about 160 km SE of Fairbanks. Image is radiometrically calibrated to a range of -26.5 to -1.0 db. The entire glacier is buried beneath the dry winter snow cover, which is transparent to the C-band SAR. The firn line from late summer 1992 is the clearly-visible boundary indicated by the arrow. See text for discussion of comparisons to field data. Image (c) ESA, 1993. Processed by K. Ahlnäs.

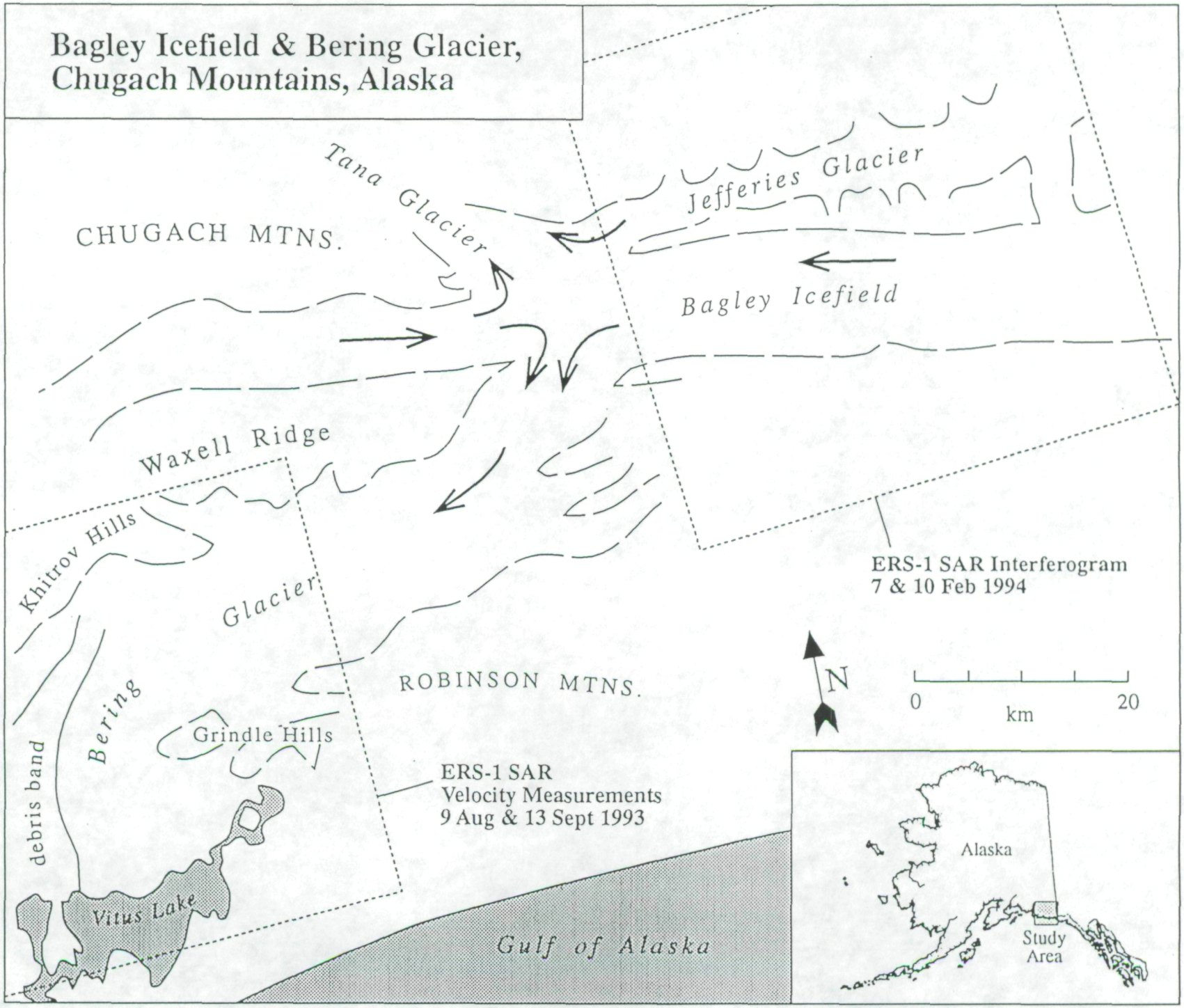

Fig. 2. Sketch map showing the Bering Glacier-Bagley Icefield area in Southcentral Alaska. Figure 3 corresponds approximately to this map area. Figures 6 & 7 are within the box close to the coast, labelled '9 Aug & 13 Sept 1993.' Figures 8 & 9 are within the more inland box labelled '7 & 10 Feb 1994.' Figures 10 & 11 are immediately west of the latter box.

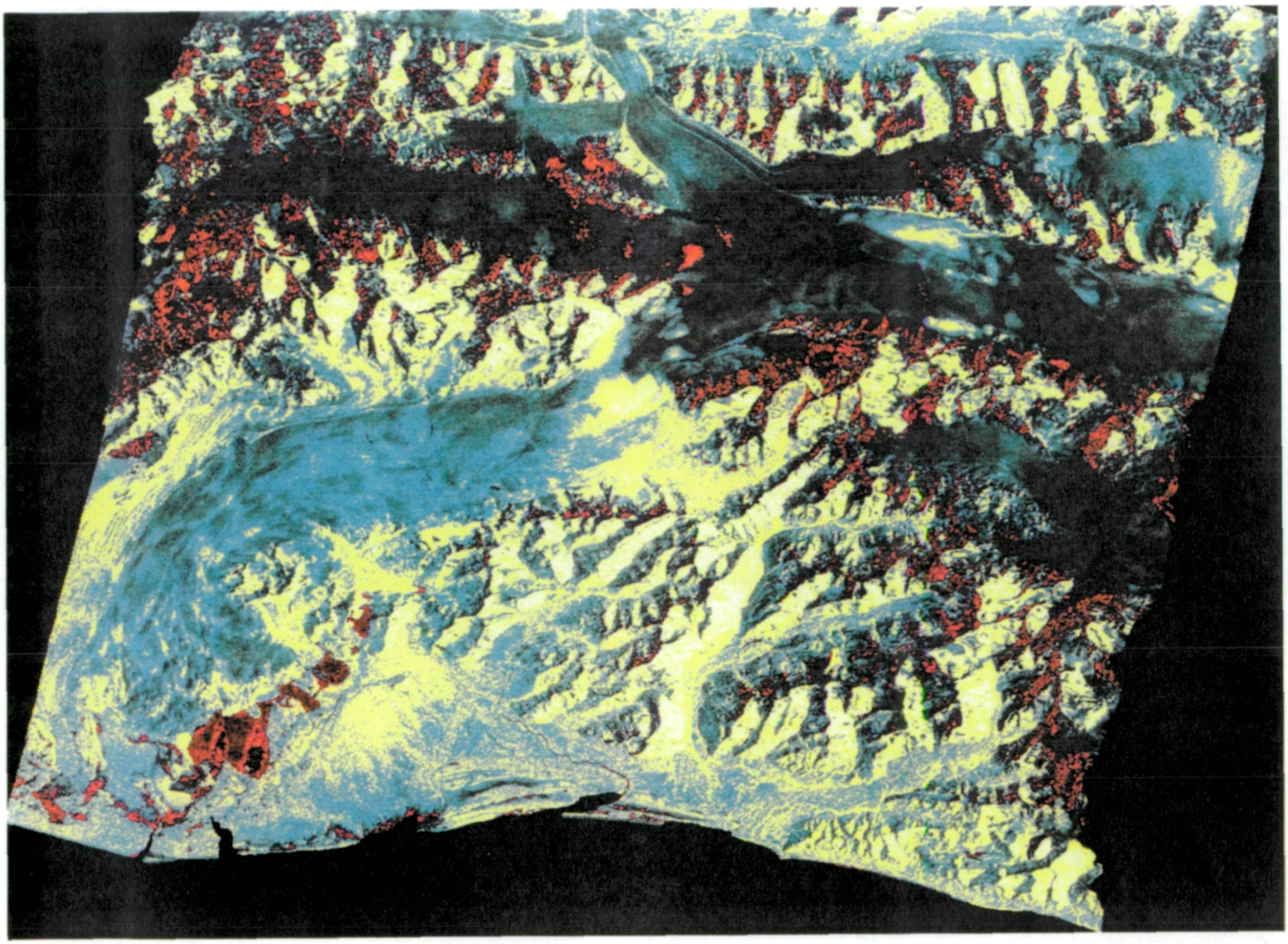

Fig. 3. Terrain-corrected low-resolution SAR image of Bagley Icefield and Bering Glacier, Alaska, acquired by ERS-1 on 9 August 1993. The image area coincides with Figure 2, approximately. Bagley Icefield, the source area for Bering Glacier, is the 8 to 12 km-wide dark linear feature extending right to left across the upper image. It is dark, i.e. specular, because wetting of the snow due to above-freezing temperatures has reduced the SAR penetration depth to near-zero. Bering Glacier, which is in a state of surge, descends from above center to lower left. The Gulf of Alaska (dark) is at bottom. The surge front reached the terminus (lower left) about three weeks after this image was acquired, during late August-early September 1993. [Terrain correction by J.J. Roush and R.M. Guritz. SAR image (c) ESA, 1993.]

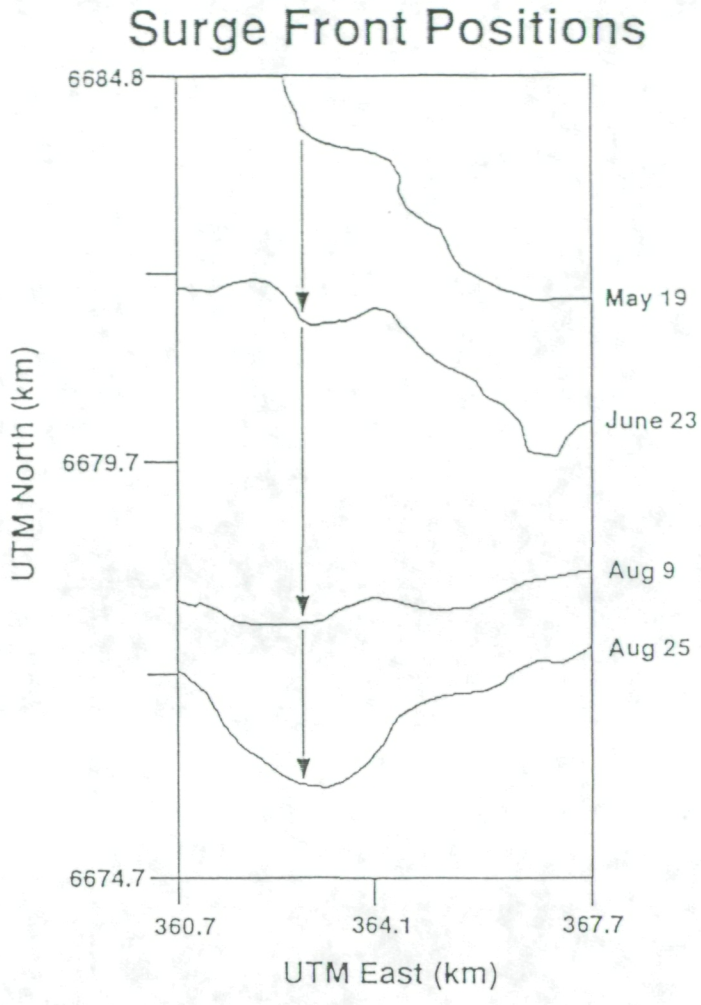

Fig. 4. Sequential positions of the surge front for an area in the lower central region of Bering Glacier, plotted in UTM coordinates. The mean rate of propagation of the surge front between 19 May and 25 August 1993, measured using subscenes of the lower glacier terrain-corrected to a pixel size of 30 m, was found by J.J. Roush to have been 90 m/day.

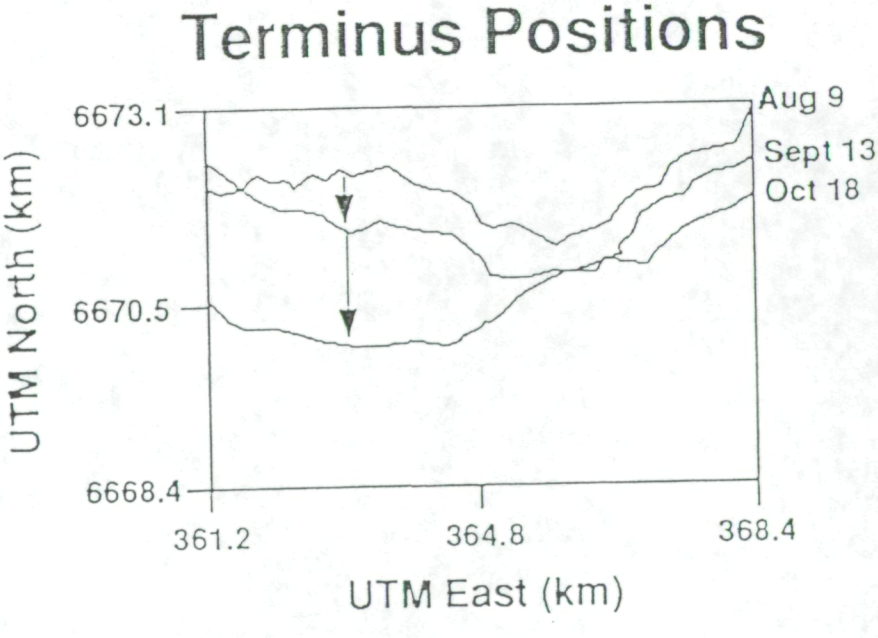

Fig. 5. Sequential positions of the terminus for the area of maximum advance in central Vitus Lake, plotted in UTM coordinates. The mean rate of advance here was found by J.J. Roush to have been 19 m/day between 9 August and 18 October 1993, using SAR subscenes terrain-corrected to a pixel size of 30 m.

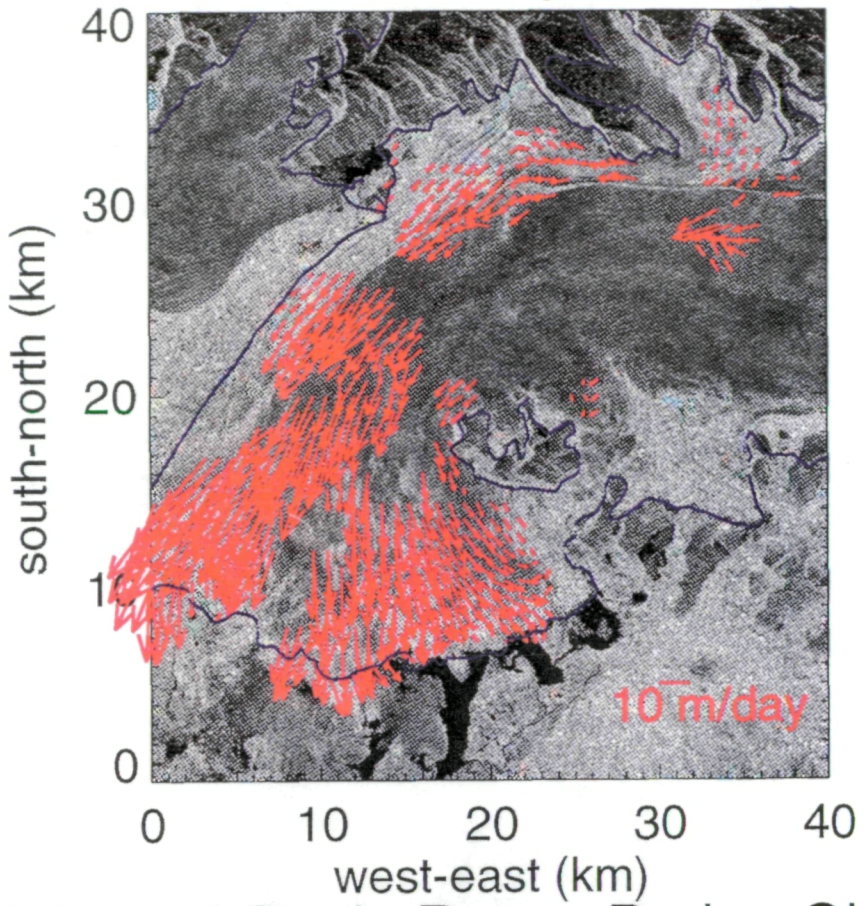

Fig. 6. Ice velocity vectors on lower Bering Glacier during the 1993-'95 surge. Two sequential images acquired from an exact repeat orbit during the 35-day orbit phase of ERS-1 were used. The image dates were 9 August and 13 September 1993, which spans the time when the propagating surge front reached the terminus. The displacements of features that could be identified in both images were measured, then converted to velocity and interpolated onto a 1 km square grid, using optimum interpolation. Many of the velocities are in the 10 to 20 m/day range. Errors are a function of pixel size and spatial interpolation distance. Only the vectors with errors less than 30% of total velocity are retained. [SAR images (c) ESA, 1993. From: D.R. Fatland, V.A. Voronina, and C.S. Lingle, 1995.]

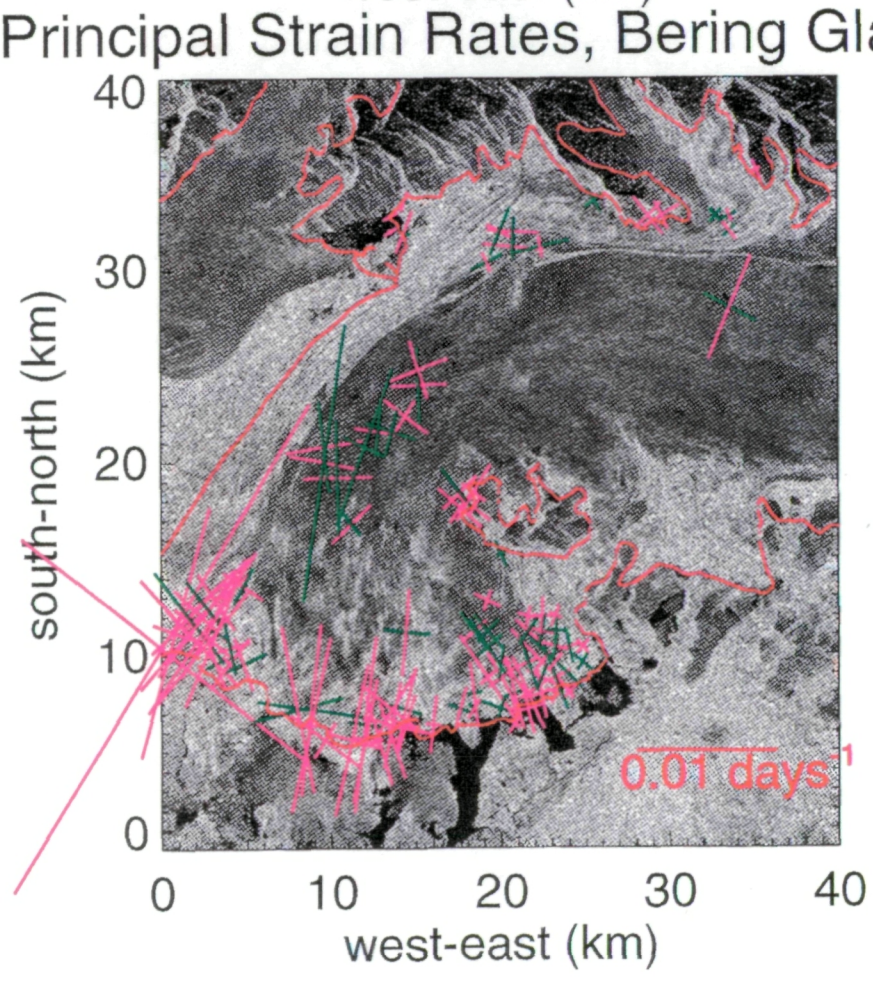

Fig. 7. Horizontal principal components of the strain-rate tensor (cross at each grid point) on the grid of Figure 6, computed by V.A. Voronina from the orthogonal gradients of the kriged velocity vectors. Red indicates compression, green extension. The complex intermingling of compression and extension can be seen which accounts for widespread orthogonal crevasse patterns and blocky seracs. Note that vertical extensive strain rates caused by thickening of the lower glacier can cause both of the horizontal principal components to be compressive. [SAR images (c) ESA, 1993. From: D.R. Fatland, V.A. Voronina, and C.S. Lingle, 1995.]

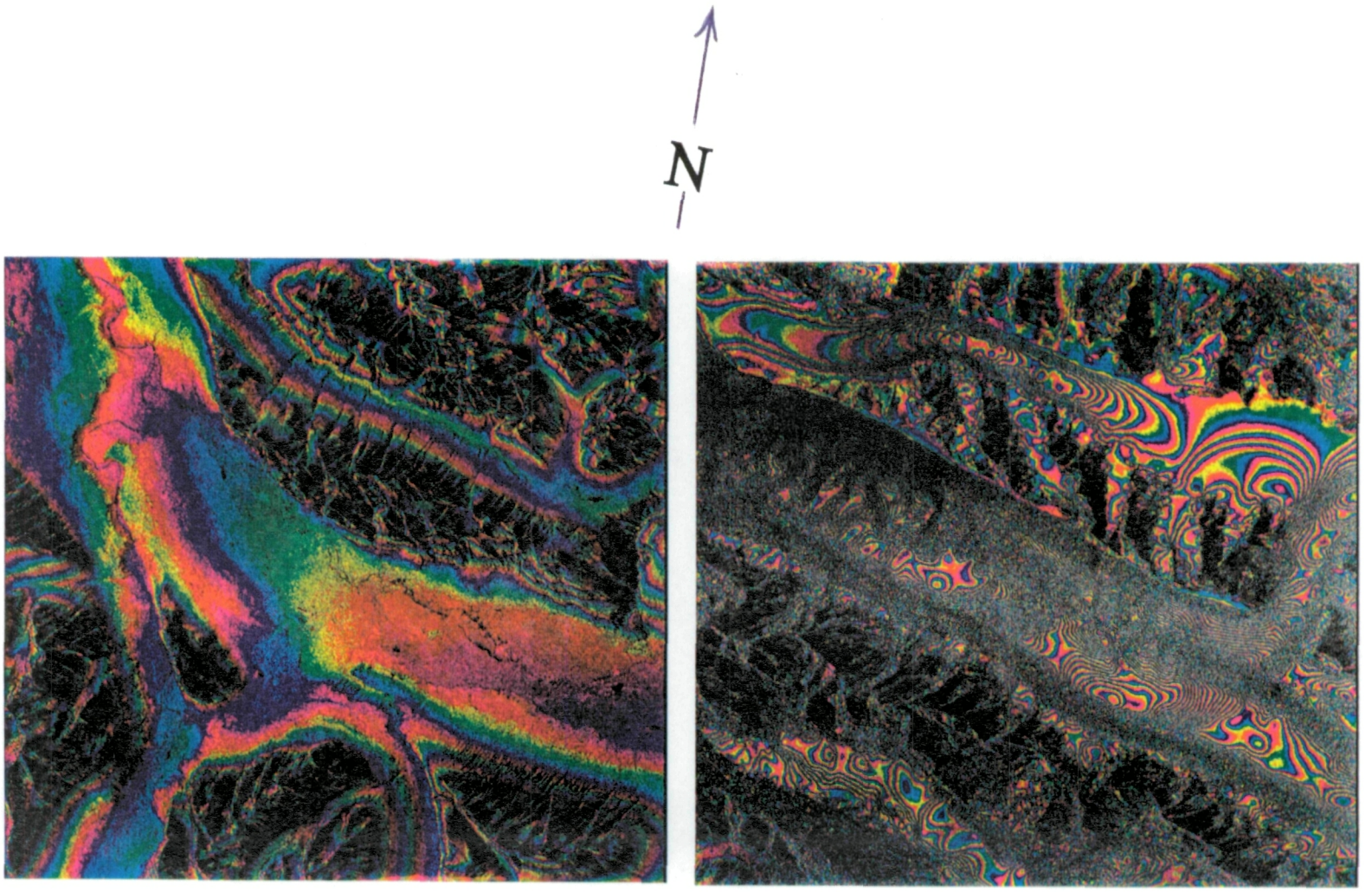

Fig. 8. Interferogram of unglacierized Chitina Valley area north (inland) of Bagley Icefield. Image pair acquired 7 and 10 February 1994, by ERS-1. Fringes represent elevation differences. Broad 'elevation fringes' throughout Chitina Valley, which curves from lower right to upper left, show that the tightly-spaced fringes in Figures 9, 10 and 11 represent ice motion, primarily, rather than topography. By D.R. Fatland. Images (c) ESA, 1994.

Fig. 9. Interferogram of Bagley Icefield (see map, Figure 2). Image pair acquired 4 and 7 February 1994, during the surge of Bering Glacier. Changes in the fringe pattern (increased decorrelation) from an interferogram synthesized prior to surge onset, in January 1992, indicate that acceleration of flow occurred within the western (left) end of the icefield segment shown here. By D.R. Fatland. Image pair (c) ESA, 1994.

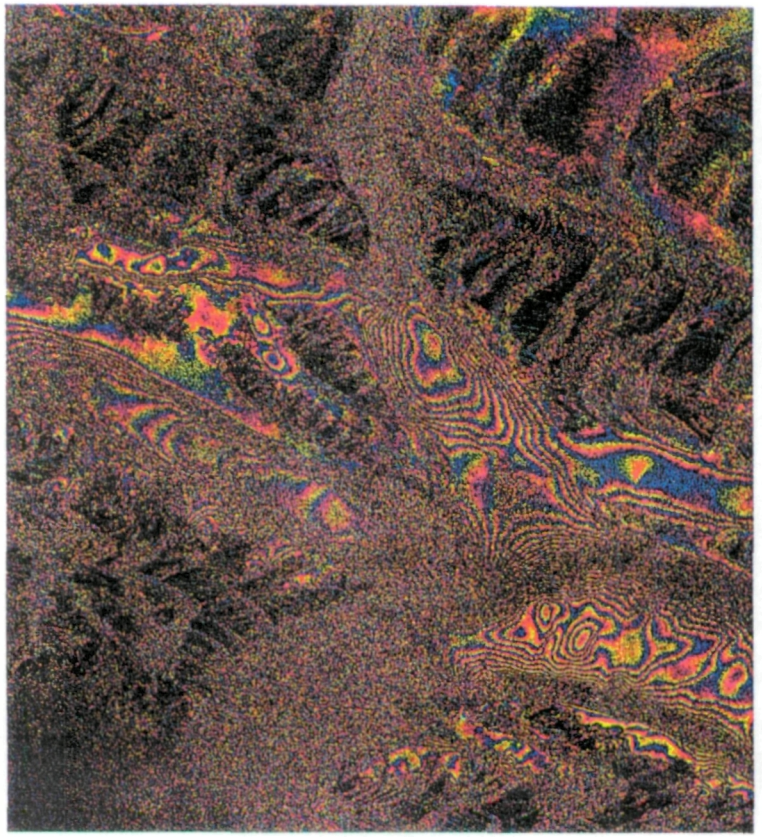

Fig. 10. Interferogram of Bagley Icefield, which is the broad 10 km-wide feature with brightly-colored fringes extending from lower right to middle left. Image pair was acquired prior to surge onset, in January 1992. Bering Glacier flows from the area below and right of center, towards lower left. Tana Glacier flows toward top-center. The bright fringes at left-center are the West Branch of Bagley Icefield, which is flowing east. The main Bagley Icefield and Bering Glacier are flowing west. The slower tributaries are characterized by broader fringes. By D.R. Fatland. SAR images (c) ESA, 1992.

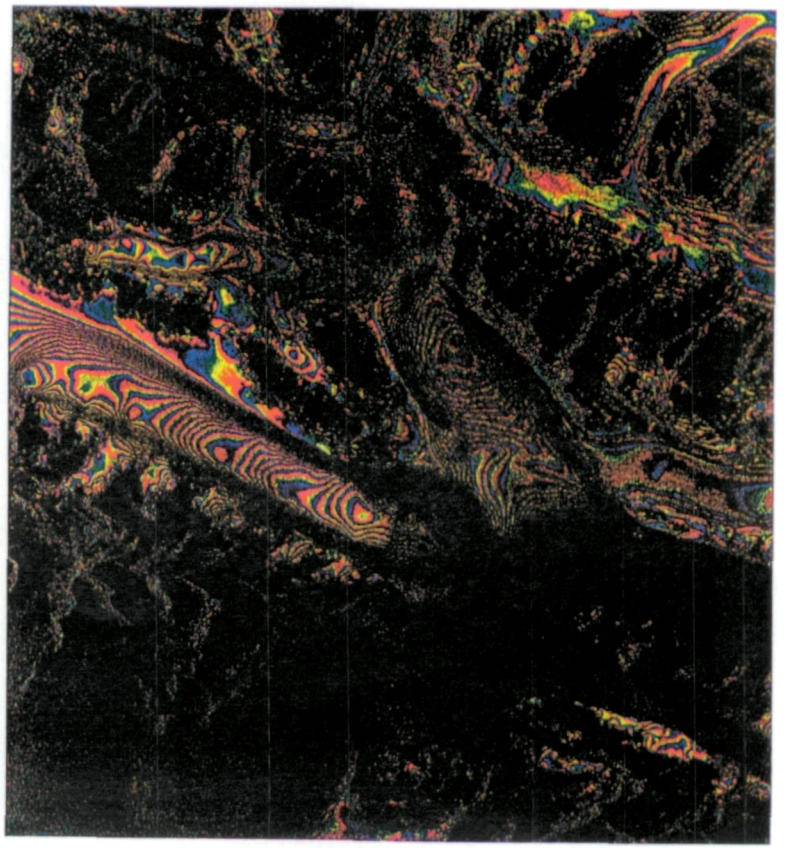

Fig. 11. Interferogram of Bagley Icefield, same area shown in Figure 10. Image pair acquired 4 and 7 February 1994 during surge of Bering Glacier. The changes in the fringe pattern at lower right show that the surge propagated up-glacier into Bagley Icefield (as well as down-glacier to the terminus). By D.R. Fatland. Image pair (c) ESA, 1994.

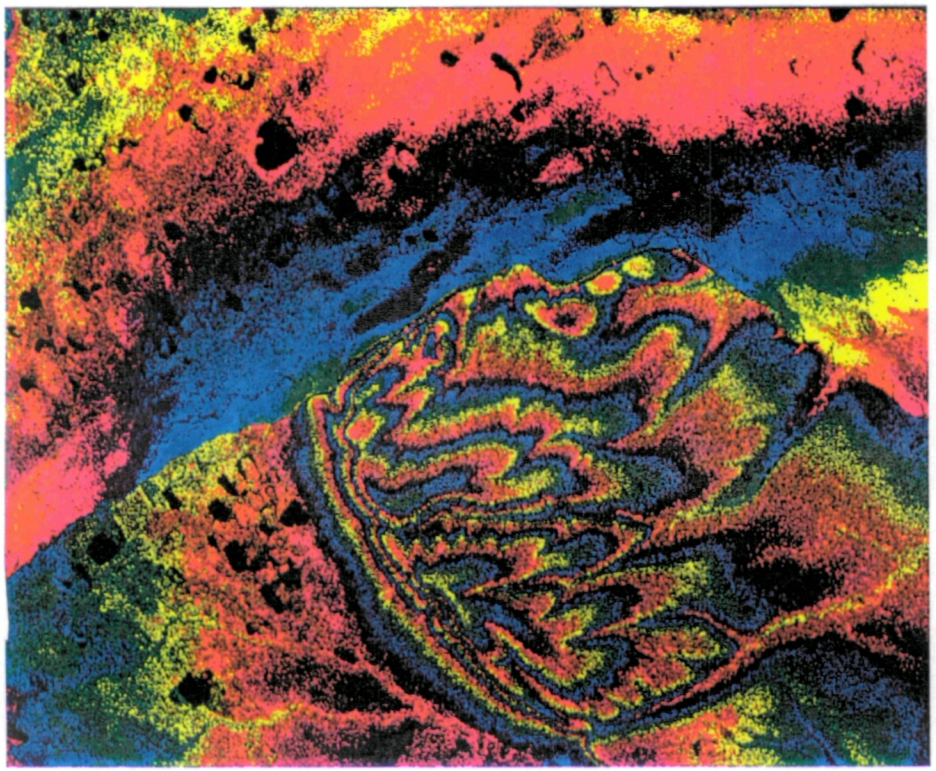

Fig. 12. Preliminary interferogram of the Franklin Bluffs area in the Arctic National Wildlife Refuge, Alaska north slope. Friges represent elevation differences. The obvious left-to-right discontinuity in the center is the Sagavanirktok River. The Dalton Highway (a.k.a. north slope haul road) and transAlaska pipeline follow the river. The figure is about 40 km E-W by 50 km N-S. By D.R. Fatland. SAR images (c) ESA, 1991.

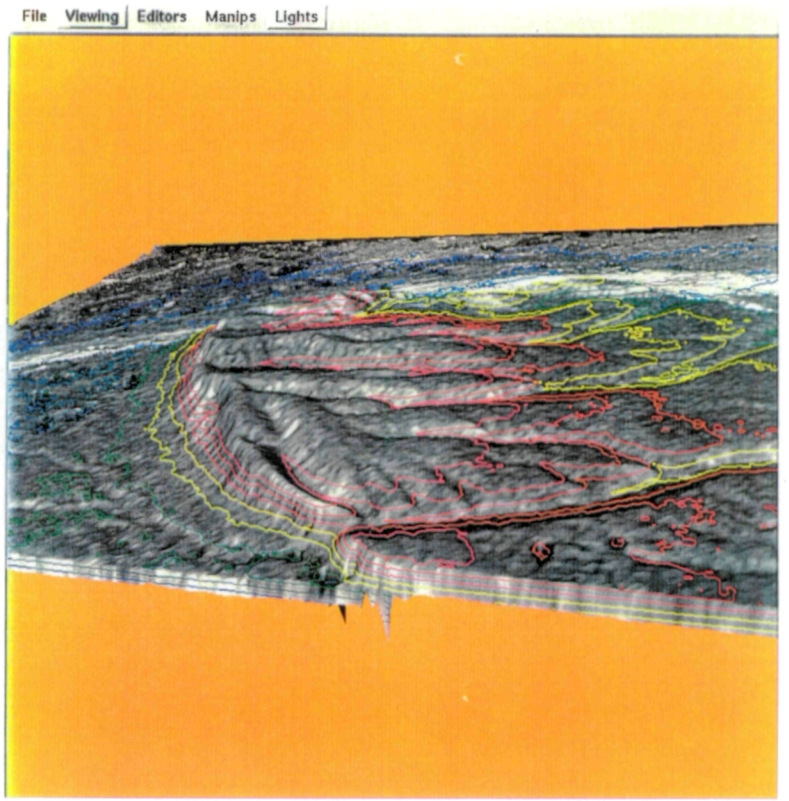

Fig. 13. Preliminary digital elevation model derived from the interferogram in Figure 12. The elevation values in this 3-D perspective rendering are defined within 160 m x 160 m pixels. The view is west; north is towards the right. Ground control consisted of control points within the corresponding 1:250,000 USGS topographic map. The Sagavanirktok River, flowing left to right, is the bright linear feature in the middle distance. The Franklin Bluffs (left foreground) are about 120 m high. By D.R. Fatland.